EARTH SURFACE PROCESSES AND LANDFORMS
Earth Surf. Process. Landforms **36**, 1105–1112 (2011)

Published online 08 March 2011 in Wiley Online Library
(wileyonlinelibrary.com) DOI: 10.1002/esp.2138

Numerical computations of a theoretical model of ribbed moraine formation

Michael Chapwanya,[1] Chris D. Clark[2] and Andrew C. Fowler[3]*
[1] Department of Mathematics and Applied Mathematics, University of Pretoria, Pretoria 0002, South Africa
[2] Department of Geography, University of Sheffield, Sheffield S10 2TN, UK
[3] MACSI, Department of Mathematics and Statistics, University of Limerick, Limerick, Republic of Ireland

Received 19 July 2010; Revised 17 January 2011; Accepted 21 January 2011

*Correspondence to: Andrew C. Fowler, MACSI, Department of Mathematics and Statistics, University of Limerick, Limerick, Republic of Ireland. E-mail: andrew.fowler@ul.ie

ESPL
Earth Surface Processes and Landforms

ABSTRACT: We develop numerical solutions of a theoretical model which has been proposed to explain the formation of subglacial bedforms. The model has been shown to have the capability of producing bedforms in two dimensions, when they may be interpreted as ribbed moraine. However, these investigations have left unanswered the question of whether the theory is capable of producing fully three-dimensional bedforms such as drumlins. We show that, while the three-dimensional calculations show realistic quasi-three-dimensional features such as dislocations in the ribbing pattern, they do not produce genuine three-dimensional drumlins. We suggest that this inadequacy is due to the treatment of subglacial drainage in the theory as a passive variable, and thus that the three-dimensional forms may be associated with conditions of sufficient subglacial water flux. Copyright © 2011 John Wiley & Sons, Ltd.

KEYWORDS: ribbed moraine; instability model; numerical computation

Introduction

Ice sheets flowing over sedimentary beds often transform what we presume to be initially fairly flat beds of glacial deposits into organized and regular patterns of undulations, having elevations of the order of 10 m and wavelengths of hundreds of metres, which are termed subglacial bedforms. The most numerous of these are drumlins, which have defied satisfactory quantitative explanation for over 100 years in spite of much effort. They are elliptically shaped streamlined hills, usually around 600 m in length, 200 m wide and less than 10 m in amplitude (Menzies, 1979; Patterson and Hooke, 1995; Clark *et al.*, 2009). Possibly genetically related to drumlins are mega-scale glacial lineations (MSGL) (Clark, 1993; King *et al.*, 2009) which are ridge–groove corrugations of much greater length (up to 100 km) than drumlins and with lateral wavelengths of hundreds to thousands of metres, but again with low amplitude (usually less than 10 m). In contrast to these bedforms which are longitudinally aligned with ice flow direction, ribbed moraines (Figure 1) are approximately parallel, fairly closely spaced ridges formed transverse to ice flow (Hättestrand and Kleman, 1999; Kleman and Hättestrand, 1999; Dunlop and Clark, 2006) and appear to resemble large ripples. All three landform types are occasionally found in close proximity to each other and sometimes grade from one type to another; classically from ribbed moraine to drumlins to MSGL in a downstream direction. For this reason it is attractive to seek a theory for the generation of these bedforms in which the different shapes are associated with different local ice sheet conditions; for example, different ice sliding velocities, or (our current preference) different subglacial water fluxes.

The motivation to seek a theoretical explanation for ribbed moraine which will also, in different parametric circumstances, produce drumlins or MSGL is apparently at odds with the alternative view that many different mechanisms may be necessary to explain these different bedforms, or even subspecies of ribbed moraine (e.g. Möller, 2006; Lindén *et al.*, 2008). For example, the transition from ribbed moraine to drumlins to lineations is only seen sometimes. More common in Sweden, for example, is an association of ribs in valleys and drumlins on high ground (Lundqvist, 1969).

While this in itself does not argue against a unifying theoretical framework, it is arguable that the sedimentological characteristics of bedforms may do so. For example, Möller (2010) argues from field studies that some southern Swedish ribbed moraines were formed by deposition of melt-out till; Lindén *et al.* (2008) suggest that some north Swedish ribbed moraines were formed as a result of subglacial folding, thrust stacking and leeside cavity deposition. However, we presume that most subglacial transverse ribs are actually true bedforms (i.e. yielding a regular patterning) and might be explained by our theory, but note that some other transverse ribs could be formed by other mechanisms such as those described by Möller (2010) or Lindén *et al.* (2008). If so, then it is of course unfortunate that we all refer to such genetically different phenomena by the common name of ribbed moraine, when in fact they might be different landforms.

The principal feature of subglacial bedforms requiring explanation is the mechanism whereby the undulations, whatever shape they may be, are created and maintained. Whether they be initiated by bedrock bumps, melt-out moraines, pull-apart drift

Figure 1. Ribbed moraine in a digital elevation model of part of Co. Monaghan in northeastern Ireland. Ice flow is from left to right, and the image is approximately 30 km across. These are extremely large ribbed moraines with downstream wavelengths of around 1 km and ridge lengths of 16 km (Clark and Meehan, 2001). More typical dimensions are wavelengths of 500 m and ridge lengths of 700 m.

sequences, remoulding of stiff till patches (Boulton, 1987), or simply through the interfacial instability of a flat bed, the bulldozing effect of an overriding ice sheet must be counteracted in some way by the combined flows of ice, sediment and water at the base.

In this paper we show that numerical solutions of a mathematical model for subglacial bedform production can generate appropriately scaled patterns that appear to resemble the surface morphology of ribbed moraines. We show that numerical computations can produce realistic ribs which have defects (e.g. planform curvature of ridges and ridge terminations and bifurcations) similar to those seen in Figure 1, and we then comment on how the theory might be developed in order to explain drumlins and MSGL within the same model.

Of all the ideas and hypotheses for subglacial bedform formation (e.g. Fisher and Shaw, 1992; Sugden and John, 1976; Hättestrand and Kleman, 1999; Lindén *et al.*, 2008), that which has been the most theoretically developed in its formulation as a mathematical model is the mechanism which causes a linear instability in the coupled flow of sediment (till) and the overlying ice, and which grows relief in the ice–till interface at preferred wavelengths to yield patterns of landforms (i.e. bedforms). The theory was originally described by Hindmarsh (1998) and Fowler (2000), and was a two-dimensional theory, thus actually describing ribbed moraine. Hindmarsh and Fowler assumed that their theory in its three-dimensional form would produce drumlins, but Schoof (2007a) suggested that this would not be true, and inferred that the theory was an unlikely candidate for the mechanism whereby subglacial bedforms form. Schoof's suggestion has been taken on as a matter of fact by Pelletier (2008), and this naturally raises the question of whether the model can generate lateral nonlinear instabilities, even though the linear theory precludes them: can a three-dimensional implementation of the instability theory model render three-dimensional bedforms?

The development of the instability model, capable of producing waveforms at the ice–sediment interface which morphometrically resemble ribbed moraine, motivated a comparison of predictions with observations. Dunlop and Clark (2006) had mapped and measured a large sample (33 000) of ribbed moraine from three different palaeo-ice sheets and in a range of glaciodynamic contexts, and reported wavelength and morphological details. These data have now been compared (primarily with regard to the wavelength, i.e. ridge spacing) with BRIE model predictions (Dunlop *et al.*, 2008) with the conclusion that the extensive suite of observations are consistent with BRIE predictions and therefore do not falsify the model.

In this paper we develop three-dimensional numerical solutions of the BRIE model in a version of the theory due to Schoof (2007a,b) and Fowler (2009). In a further development of the results of Dunlop *et al.* (2008), Fowler (2009) showed that amplitudes of the correct magnitude could also be predicted, but his results were restricted to purely two-dimensional waveforms. One possibility, suggested by Fowler (2009), was that the finite-amplitude two-dimensional waveforms of the instability theory might have secondary transverse instabilities, thus forming drumlins. Part of our purpose in this paper is to examine this question, to establish the degree to which the instability theory thus far developed is capable of producing three-dimensionality, whether in the form of fully formed drumlins, or simply the dislocated two-dimensional shapes seen in Figure 1.

Mathematical Model

We present here a recent version of the instability theory, based on work by Fowler (2010b). Earlier versions of the theory represent particular simplifications of this, as we will try to indicate.

The basic geometry we consider is shown in Figure 2. We take coordinates (x, y, z) with z vertical. The ice upper surface is at $z = z_i$ and slopes gently in the x direction (hence driving ice flow from left to right, as well as a subglacial water flow, as we assume the bed is at the melting point, and there is a subglacial melt-produced water flux). At the origin $x = 0$, we suppose that the depth is d_i in the unperturbed state where ice flows over a flat till sheet. We define N to be the effective normal stress at the ice base $z = s$. Fowler (2010b) shows that there is a consequent hydraulic head

$$\psi = p_w + \rho_w g s - (p_a + \rho_i g d_i) \tag{1}$$

and when written in terms of the effective stress, this is

$$\psi = \rho_i g (z_i - d_i) + \Delta\rho_{wi} g s + \Pi - \tau_{nn} - N \tag{2}$$

where p_w is water pressure, ρ_i is ice density, $\Delta\rho_{wi} = \rho_w - \rho_i$ is the difference between water and ice densities, Π is the reduced (by subtraction of the cryostatic value) pressure, and τ_{nn} is the deviatoric normal ice stress at the ice base.

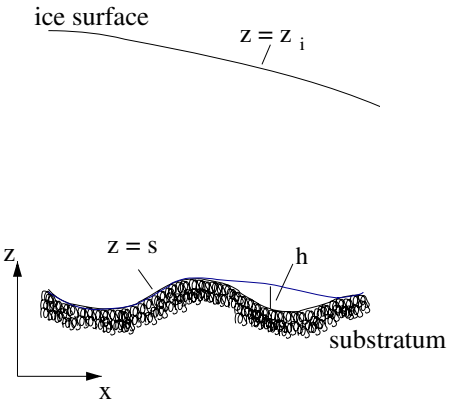

Figure 2. Basic geometry of the flow. The ice base is at $z = s$, and this is also the till surface, unless the ice separates from the bed. If that happens, in a stream or a cavity, the water depth is h, the ice base is at $z = s$ and the till surface is at $z = s - h$. In the present paper, we suppose that till can be squeezed into cavities, so that in effect $h = 0$ everywhere.

When the ice is attached to the till surface, i.e. the water depth h is zero, then we model the groundwater flow in the till by Darcian flow:

$$\varphi_t = \frac{k_p}{\eta_w}\nabla^2\psi \tag{3}$$

where we ignore local melt production. Here φ is the till porosity, k_p is the till permeability of the till, and η_w is the viscosity of water.

The sediment motion is described by the Exner equation:

$$s_t + \nabla.\mathbf{q} = 0 \tag{4}$$

where the sediment flux is

$$\mathbf{q} = A\mathbf{V},\ \mathbf{V} = c\mathbf{u} - b\nabla p_e \tag{5}$$

p_e is the effective pressure in the till,

$$p_e = N + \rho_T g(s - z) \tag{6}$$

ρ_T is the density of till, and the depth of deformable till A is given by

$$A = \frac{[\tau - \mu N]_+}{\mu\Delta\rho_{sw} g(1-\varphi)} \tag{7}$$

where μ is a coefficient of friction for the sediment, $\Delta\rho_{sw} = \rho_s - \rho_w$ is the difference in density between sediment and water, and the divergence and gradient operators are horizontal, i.e. with respect to x and y only. The average till velocity $\mathbf{V}$ represents the motion due both to shearing by the ice velocity $\mathbf{u}$ and squeezing down gradients in effective pressure.

We suppose that the porosity of till is described by a dependence on effective pressure p_e, so that $\varphi_t = \varphi'(p_e)\frac{\partial p_e}{\partial t}$. Assuming that $\varphi' < 0$ is constant, and that the aquifer depth, permeability and porosity do not vary significantly, Fowler (2010b) shows that Equation (3) leads to

$$\varphi'[N_t + r_a\rho_T g s_t] = \frac{k_p}{\eta_w}\nabla^2\psi \tag{8}$$

where $r_a \in [0, 1]$ is a parameter which represents an uncertainty in the depth of the groundwater aquifer. If the aquifer is in the whole sediment column $0 < z < s$, then $r_a = 1$, while if it is confined to a fixed depth of dilatant till beneath the ice/till interface, then $r_a = 0$.

When the model (2), (4), (5), (7) and (8) is made dimensionless (Fowler 2010b), we obtain the equations in the form

$$\begin{gathered}\psi = -\sigma x + s - \Theta - N,\\ N_t + r'' s_t = -\Gamma\nabla^2\psi,\\ s_t + \nabla.[A\{c\bar{u}\mathbf{i} - \beta\nabla(N + r's)\}] = 0,\\ A = \left[\frac{\tau}{\mu} - N\right]_+,\ \tau = f(\bar{u}, N)\end{gathered} \tag{9}$$

The definition of τ is determined by the sliding law. In addition, the ice surface perturbation H from the constant slope surface is determined by

$$\lambda H_t = \Xi \tag{10}$$

and the quantities Θ and Ξ are themselves determined in terms of the quantities H, K and F, where the latter two are defined by

$$K = \alpha s_t + \bar{u}s_x,\ F = f(\bar{u}, N) - 1 \tag{11}$$

The determination of Θ and Ξ is described by Fowler (2010a). The Fourier transforms of Θ and Ξ are given by linear combinations of those of H, K and F.

The definitions of the parameters in the model are given by Fowler (2010b), along with typical representative values; these are given in Table I.

A feature of the model is that when N reaches zero the ice must separate from the bed, forming a cavity or a stream. Fowler (2010b) describes an appropriate model for water and sediment transport in this case. Here we adopt the simpler approach of Fowler (2009), which simply allows A to take any positive value when $N = 0$. The extended function $A(N)$ thus defined is then approximated as described below in determining solutions.

Numerical Simulations

In this section, we present numerical solutions of two different versions of the model in Equation (9). In earlier work (e.g. Fowler, 2010a), the subglacial hydraulic system was taken to be static, in

Table I. Typical values of the dimensionless parameters

Symbol	Description	Parameter value
	Physical parameters	
β	Lateral till flux diffusivity	1.26×10^{-3}
r'		24.1
r''		≤ 24.1
θ	(static streams)	0.38
θ	(dynamic streams)	1
Γ	(dynamic streams)	0.073
b	Sliding law parameter (< 1 for instability)	0.6
s_-	Stream level	0
λ	Timescale for surface adjustment	0.8×10^{-2}
α	Deformable till depth parameter	0.1
σ	Corrugation	0.2
	Numerical parameters	
ω	Controls slope in $A(N)$	2.0
δ	Controls approach to $N = 1$ in $A(N)$	0.1
γ	Controls severity near $N = 0$ in $A(N)$	2.0
D	Filtering coefficient	0.2
m	Fourier modes	120
n	Grid points	400

the following sense. The water pressure at the ice/till interface was supposed to be hydrostatically linked to a stream system, whose effective pressure was supposed determined independently by a hydraulic model such as that of Röthlisberger (1972) or Walder and Fowler (1994), which provided a prescription for the effective pressure near the channel:

$$N_c = p_a + \rho_i g(z_i - s_-) - p_c \tag{12}$$

where p_c is the channel water pressure and $s_-(t)$ is its elevation. This led to a prescription for N in dimensionless form as

$$N = 1 - s_- + s - H - \Theta \tag{13}$$

where the stresses are scaled with N_c, and the ice flow coefficients Θ and Ξ then depend on the additional parameter

$$\theta = \frac{\tau_b}{N_c} \tag{14}$$

The coefficient 1 in Equation (13) indicates the assumption that N_c is constant. In terms of ψ (as scaled in Equation (9)), i.e. with the ice sheet basal stress τ_b (see Fowler, 2010b), (Equation (12)) is equivalent to

$$\psi_c = -\sigma x + s_-(t) + H - \frac{1}{\theta} \tag{15}$$

Consulting Equation (9), we see that the hydrostatic limit corresponds to $\Gamma \to \infty$, in which case (with appropriate boundary conditions) we might suppose

$$\psi = -\sigma x + s_-(t) - A \tag{16}$$

where A is constant. This can be reconciled with Equation (15) if we assume $N_c = (A + H)\tau_b$, but in reality we should not worry about any discrepancy, since in the model (9) there is no explicit recognition of a separate stream system. In fact, as we will find $H \sim 10^{-3}$ and $A \approx \theta^{-1} \approx 2.5$, there is very little difference. Thus we will consider the model in two forms: the first is the static stream system in which we replace the first two equations in (9) by (13) (and we have a prescribed constant N_c, and thus the parameter $\theta \neq 1$); the second, which we call a dynamic stream system, solves Equation (9) with $\Gamma < \infty$; there are no explicit streams present, and thus N_c has no meaning. In terms of the scaled ice model, this means that we choose $\theta = 1$, and the stresses are scaled with τ_b.

Passive stream model

In this section we present a numerical solution to the dimensionless equations governing the evolution of the ice–till interface $s(x, y, t)$, basal effective pressure $N(x, y, t)$, and ice surface $H(x, y, t)$. Both the bed s and the upper surface H require initial conditions, and these are taken to correspond to small-amplitude perturbations of the uniform flat state. Specifically, s is given by a random function of dimensionless amplitude $\sim 10^{-3}$, while H is taken to be flat, i.e. $H = 0$. Because the calculation of the ice flow is done using Fourier transforms (Fowler, 2010a), it is particularly convenient to use a spectral method. Denoting the transforms by overhats, we take the Fourier transform of Equations $(9)_3$, (10) and (13) to get

$$\begin{gathered} \hat{s}_t = ik_1 c\bar{u}\hat{A} - \beta k^2 \hat{N}, \\ \hat{N} = \hat{1} + \hat{s} - \hat{s}_- - \hat{H} - \hat{\Theta}, \\ \lambda \hat{H}_t = \hat{\Xi} \end{gathered} \tag{17}$$

where $\mathbf{k} = (k_1, k_2)$ and $k = |\mathbf{k}|$. A further simplification has been made in $(17)_1$, in that the diffusion coefficient βA for N is replaced by the constant β. Here $\hat{\Theta}$ and $\hat{\Xi}$ are linear functions of $\hat{H}$, $\hat{F}$ and $\hat{K}$; see Fowler (2010a). For convenience we take $\bar{u} = 1$ and $c = 1$. To close the system, we first specify the sliding law (as given by the generalized Weertman law):

$$f(1, N) = \theta N^b \tag{18}$$

and secondly, we specify the functional dependence of $A(N)$. Following Fowler (2009) we approximate $A(N)$ via

$$A(N) = \left[\delta\left\{\frac{1}{N^\gamma} - 1\right\} + N^\omega(2 - N)\right]_+ \tag{19}$$

for some constants δ, γ and ω.

The computational domain is taken to be a square with periodic boundary conditions, i.e. the variables are taken to be periodic over the domain. Since the domain is much larger than the waveforms which develop, this is not a constrictive assumption. Unless otherwise noted, the domain is discretized with 400×400 points in the physical space and utilize 120×120 Fourier modes. As for the initial conditions, we consider a perturbed ice–till interface with an amplitude of approximately 10^{-3} units and a uniform ice surface H. The integration is performed in the spectral domain and we invert to recover the solution. All of the solutions were performed on a 3 GHz, Intel Core 2 Duo CPU, 3.25 GB RAM, with a typical run requiring approximately 12 hours of computation time.

The solution behaved in a way consistent with Fowler's (2009) observations: there is an initial phase where N grows in amplitude, oscillating about $N = 1$ on the unstable branch of the $A(N)$ curve. However, in the present case these oscillations are so severe that there is a breakdown in the integration. This suggests taking very small time steps or using some adaptive time-stepping method. Hence, in addition to reducing the time step, we filtered the transforms via pre-multiplication by

$$r = \frac{1}{1 + Dk^2} \tag{20}$$

where D is a small filtering coefficient (Fowler, 2009). This reduces the oscillations in N.

The equations are integrated to an approximately stationary state, as shown in Figures 3–5. The side profiles are consistent with Fowler's (2009) filtered two-dimensional simulations. Discussion of these results is given below.

Active stream model

In this section we present numerical solutions of the dynamic stream model (Equation (9)). We put

$$\psi = -\sigma x + \Psi \tag{21}$$

and then take Fourier transforms to find (again taking constant diffusivity for N)

$$\begin{gathered} \hat{N}_t + r''\hat{s}_t = \Gamma k^2 \hat{\Psi}, \\ \hat{s}_t = ik_1 c\bar{u}\hat{A} - \beta k^2\left(\hat{N} + r'\hat{s}\right), \\ \hat{\Psi} = \hat{s} - \hat{\Theta} - \hat{N} \end{gathered} \tag{22}$$

where all the parameters are chosen as in Fowler (2010b).

Here we consider a computational domain of size 10 dimensionless units in each direction. The domain is discretized

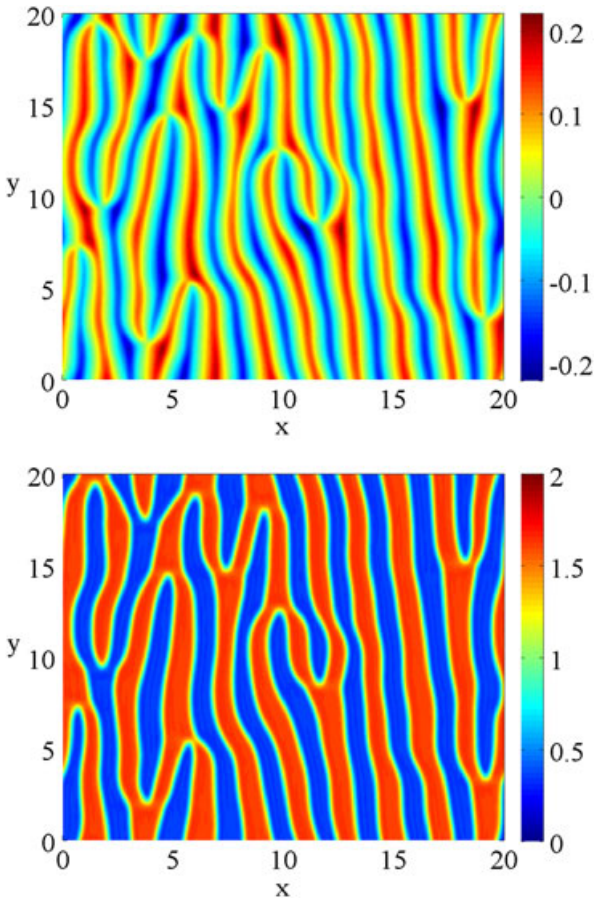

Figure 3. Profiles for the ice base and effective pressure for the static stream system, with all the parameters chosen as in Table I. Ice flow is from left to right. The final state was reached at $t \approx 5$. The bedforms are essentially two-dimensional, with numerous dislocations. The blue areas in the right-hand figure are cavities, where N is (close to) zero. The units are dimensionless; thus the horizontal lengths are measured in units of $l \approx 280$ m, while the elevation colour scale is in units of $d_D \approx 12$ m. These scales themselves depend on ice flow properties, and will not necessarily always take these values. Thus in the figures here the total elevation of the bedforms is about 5 m, while their period is about 620 m. (Upper) Profile for the ice base, s. (Lower) Profile for the effective basal pressure, N.

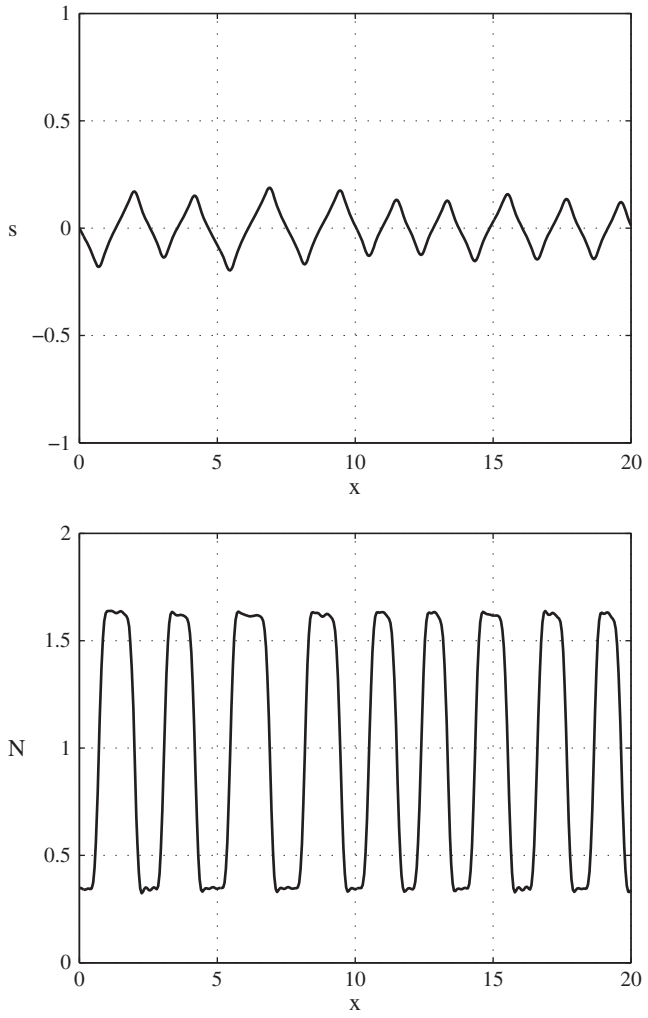

Figure 4. Side-view profiles corresponding to Figure 3 taken at $y = 0$. (Upper) Profile for the ice base, s. (Lower) Profile for the effective basal pressure, N.

on a uniform mesh with 200 grid points and 60 Fourier modes in each direction. The numerical simulations are presented in Figures 6–8.

While the numerical computations for the passive case seemed relatively benign, this was less true of the active case. There was a numerically suspicious tendency to form 'boomerangs', which are manifested as fairly sudden right-angled turns in the topographic contours. Figure 6 is a fairly representative example, where a typical boomerang can be seen at $(6.5, 5.5)$ and $(7, 7)$, for example. These boomerangs tend to propagate through the pattern, suggesting that, if real, they may be transient effects.

The main distinction in the active case is that the ribs now move in the direction of ice flow and are no longer stationary features. In addition, the ribs coarsen as they develop, in keeping with models of other similar phenomena, for example desert dunes.

Numerical diagnostics

To ensure our numerical algorithm is computing a consistent solution, several numerical experiments were performed.

To investigate the accuracy and efficiency of the numerical algorithm, different methods were used to integrate the resulting Fourier discretizations. These include the forward Euler (FE) method, the modified Euler (ME) (or Crank–Nicolson) method and the classical fourth-order Runge Kutta (RK4) method. However, finally we resorted to the built-in MATLAB ODE solvers because of their simplicity and adaptive time step capability. In particular, we encountered stability problems using the FE method and simulations with ME or RK4 were only possible with time steps as low as 10^{-5}. We emphasize that we observed no differences in the resulting solutions from all four methods considered.

To investigate the effects of the initial condition on the final state profile, we ran the simulations with different initial conditions. For example, we used the final state solution as our initial condition but with double the number of Fourier modes. A related test involved integrating the equations over a larger time domain. In all cases there were no observed discrepancies in the final solution profile.

A particular question of interest involved the effect of varying the ice thickness through the parameter σ. Results (not shown here) indicate that the wavelength of the ribs is larger for deeper ice (smaller σ).

Discussion

We have considered a spectral method to solve a theoretical model of ribbed moraine formation in three dimensions. The challenge of using spectral approximations to solve equations

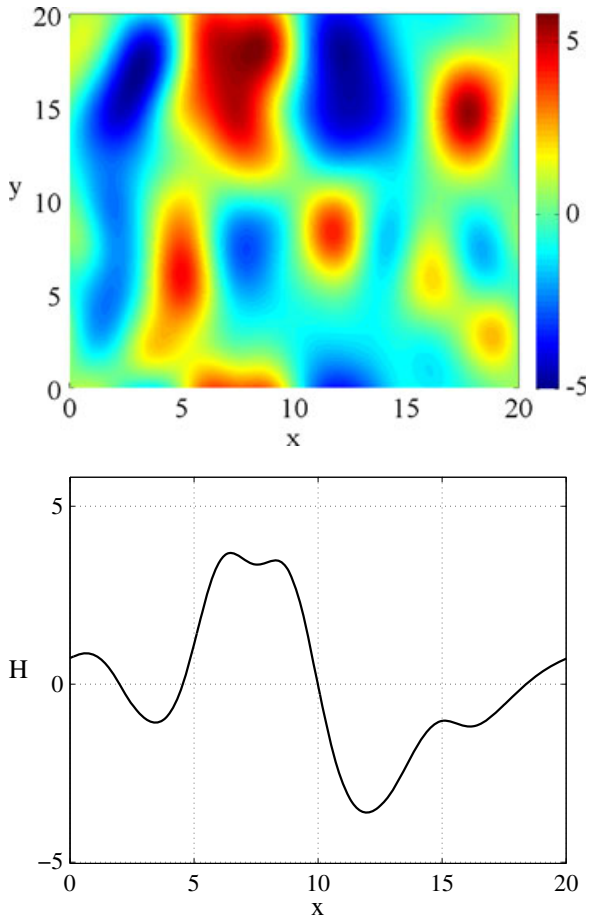

Figure 5. Profiles for the ice surface. Units scaled up by 10^3. The final state was reached at $t \approx 5$. (Upper) Profile for the ice surface, H. (Lower) Side-view profile for the ice surface at $y = 0$.

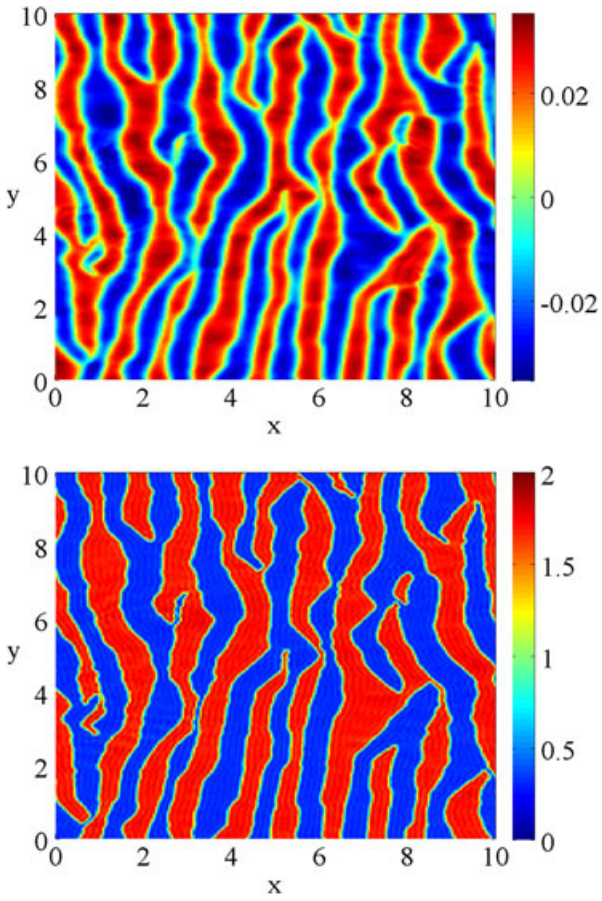

Figure 6. Computations of the dynamic stream system on a 10×10 domain: profiles for the ice base and effective pressure with all the parameters chosen as in Table I, except that $\sigma = 0.28$ and $\alpha = 0.086$, and we take $r'' = r'$. The steady state was reached at $t \approx 2$. (Upper) Profile for ice base, s. (Lower) Profile for effective basal pressure, N.

that exhibit piecewise smooth solutions has been encountered elsewhere (Fowler, 2009; Canuto *et al.*, 2007) and is well known in the spectral methods community. In most cases some smoothing mechanism has to be implemented. In the present case, the computations break down if the time step is too large, as in that case N takes negative values. Thus a filtering procedure was applied at every time step to dampen the spurious high-frequency oscillations which occur because of Gibbs' phenomena. Different filtering coefficients were used to test the converged numerical solution and in all cases there was no discernible difference in the solutions so obtained.

The theoretical model is a generalization of that of Fowler (2009), in which it was assumed that the basal water in the till was in hydraulic equilibrium, and where cavities produced by the flow of ice over the developing topography were supposed to be infilled by sediment, in the manner of crag and tails. This assumption leads to a formulation in which the deformable till thickness $A(N)$ takes on arbitrary (positive) values if N reaches zero, and in the numerical implementation this formulation is approximated by taking the function $A(N)$ to be as defined in Equation (19).

Additional developments in the model are consideration of finite depth of ice, which allows a prescription for the perturbation to the ice upper surface, the incorporation of a term which describes the squeezing of till down effective pressure gradients, which leads to a diffusive term $\nabla^2 N$ in the Exner equation, and an allowance for non-equilibrium hydraulic potential, which leads to a diffusive equation for the hydraulic potential ψ, with a diffusional coefficient Γ. The equilibrium limit, in which $\Gamma \to \infty$, is termed the static stream model, while that in which Γ is finite is termed the dynamic stream model. Both models are able to produce rib-like formations, but over similar timescales these have distinct forms.

The static stream model ribs ($\Gamma = \infty$) reach an apparent steady state on a timescale of $O(1)$, dimensionally corresponding to 30 years. The ribs are characterized by regular waveforms (Figure 3) in which dislocations occur through the branching and coalescence of individual ridges. The waveforms (Figure 4) are unrealistic, having sharp jumps at peak and trough, associated with the end points of the cavities. Mathematically, the reason for this is that where N jumps rapidly (at the end points of cavities) the term ∇N in Equation $(9)_3$ becomes large, and so ∇s has to jump rapidly also.

The corresponding perturbation to the ice surface is shown in Figure 5. It is noticeable that the rib wavelength is more or less absent in the surface perturbation, and also that the amplitude is of $O(10^{-2})$; the scale for this is $d_i S$, where d_i is the ice depth and S is the ice surface slope. With $d_i = 1000$ m and $S = 10^{-3}$, the ice surface perturbation scale is 1 m, so that Figure 5 suggests surface perturbations of order 1 cm: essentially nothing.

The corresponding contour plots for s and N in the dynamic stream model with $\Gamma = 0.073$ at a similar time ($t = 2$, corresponding to 60 years) are shown in Figure 6. These ribs are much more reminiscent of real ribbed moraine, both in planform and in profile (Figure 7), and this can be emphasized by plotting the elevation data as if it were a digital elevation model, as shown in Figure 9. However, there is a caveat. It can be seen that their amplitude is much smaller (corresponding to

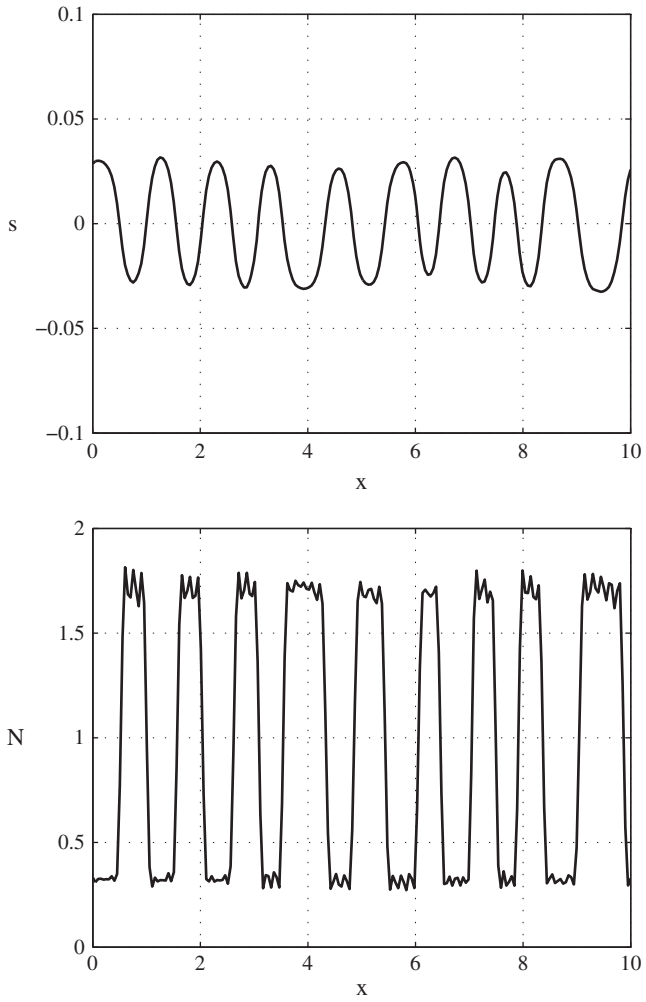

Figure 7. Computations on a 10×10 domain of the dynamic stream system: side-view profiles for Figure 6 taken at $y = 0$. (Upper) Profile for ice base, s. (Lower) Profile for effective basal pressure, N.

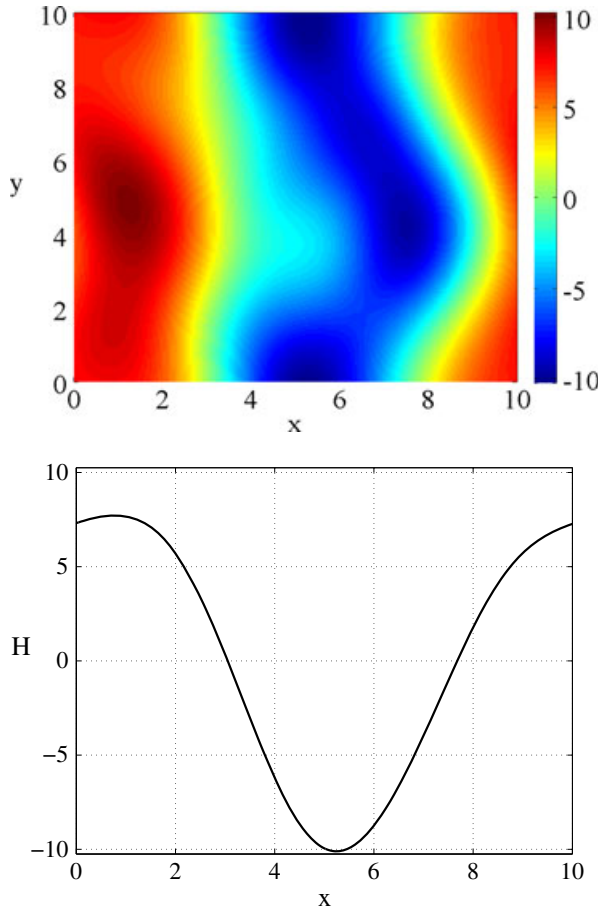

Figure 8. Profiles for the ice surface. Units scaled up by 10^3. (Upper) Profile for the ice surface, H. (Lower) Side-view profile for the ice surface at $y = 0$.

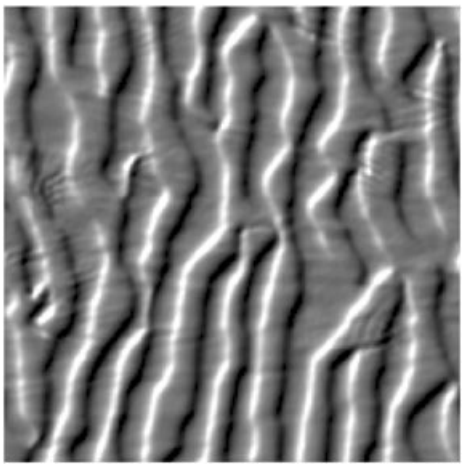

Figure 9. The surface topography of ribs from the model run of Figure 6, with a solar-shaded rendition typically applied to digital elevation models of real landscapes. The modelled ribs have the appearance of ribbed moraine when seen in digital elevation models (e.g. Figure 1). The appearance of channel-like forms breaching some of the ribs should not be taken seriously as they are likely artefacts; the model does not resolve water routing at this scale.

about a metre), and in addition they migrate downstream, becoming coarser as they do so. Our inference is that this is due to the fact that Γ is small in Equation (22), which has the effect of allowing the hydraulic potential to evolve over the longer timescale $O\left(\frac{1}{\Gamma}\right)$, which corresponds to about 400 years. Indeed, the steady state solutions shown in Figure 3 are also solutions of the dynamic stream model, although it is not obvious that they will be stable. To examine this, we ran the dynamic stream model to a dimensionless time $t = 30$. It is found that the ribs continue to propagate and coarsen, suggesting that the statically determined ribs in Figure 3 are unstable.

Although the ribs in Figure 6 are very suggestive of real ribs, one must be circumspect about the model that has been used to produce them. Both the dynamic and static stream theories assume a background hydraulic system with, in effect, very little water flux. Fowler (2010b) shows that for a subglacial system with no explicitly separated water flow (i.e. $h = 0$ everywhere), a typical steady state value of the dimensionless hydraulic gradient would be $-\psi_x = \Omega \sim 10^6$, assuming till permeability of 10^{-15} m^2. Such a large value of the hydraulic gradient is not consistent with the present model, although excavation of fines near the ice/till interface can effectively increase the permeability while still allowing ice to maintain contact with the coarser sediments (Creyts and Schoof, 2009). Even in this case, however, we would expect water to be concentrated in the cavitated (blue) regions in Figure 6b, and it is evident from this figure that the ribs themselves provide an effective barrier to downstream water flow. This suggests that if the magnitude of the water flux is incorporated into the model, it will alter the morphology of the ribs; another way of putting this is to say that we would only expect figures such as those in Figure 6 to occur where the subglacial water flux is small: this would be near

divides, or near regions where the basal ice is subtemperate (i.e. at the melting point, but with no net production of water).

A further point is that the timescale for evolution of the ribs in Figure 6 is so long that it is reasonable to suppose that changes in ice flow or thermal regime will effectively cause the boundary conditions for the dynamic stream model to vary on the timescale $O\left(\frac{1}{\Gamma}\right)$, so that transient solutions such as that in Figure 6 would indeed be realistic.

The instability theory, in so far as we have developed it, does not yet say anything about the subsurface sediment architecture. Our aim has been to use a physically based theory to explain the surface undulations that comprise ribbed moraine, because we regard this to be the primary characteristic of such landforms. The classical sedimentological approach tends to take a different view, arguing that the nature and disposition of the internal sediments are the primary characteristic, and conceptual models are then built to explain these (e.g. Möller, 2010; Lindén *et al.*, 2008), but thus far they appear unable to explain the regular patterning of ribbed moraine. Clearly, at some point both approaches need also to attempt to explain the other aspect. How the instability theory might explain sediment architecture will be reported in forthcoming publications.

Conclusions

Three-dimensional calculations of two versions of the instability theory of drumlin formation suggest that the segmented ridge pattern which is typically observed can be well simulated by the model. However, no genuine three-dimensional bedforms (drumlins) are produced. In both versions of the model presented here, it is essentially assumed that hydraulic drainage occurs through a passive stream system which does not interact with the ice flow. Two versions of this theory are studied: a static one, where water is everywhere in hydraulic equilibrium, and a dynamic one, where transient effects due to groundwater flow are included. Elsewhere (Fowler, 2010b), we have shown that if an active stream flow model is included then rilling instabilities occur which cause the formation of down-ice water streams separated (at scales of hundreds of metres) by elevated lineations. It is therefore natural to expect that if an active stream system is included in the model then the ribbing and rilling instabilities will combine to form genuine three-dimensional bedforms, and it is also natural to suppose that the particular shape of these will be determined by the size of the basal water flux through the system. A systematic investigation of this awaits further work.

Acknowledgements— M.C. and A.C.F. acknowledge the support of the Mathematics Applications Consortium for Science and Industry (www.macsi.ul.ie) funded by the Science Foundation Ireland mathematics initiative grant 06/MI/005. A.C.F. and C.D.C. acknowledge the support of NERC grant NE/D013070/1, testing the instability theory of subglacial bedform production. For continuing fruitful discussions, our thanks to Chris Stokes, Felix Ng, Matteo Spagnolo, Paul Dunlop and Richard Hindmarsh.

References

Boulton GS. 1987. A theory of drumlin formation by subglacial sediment deformation. In *Drumlin Symposium*, Menzies J, Rose J (eds). AA Balkema: Rotterdam; 25–80.

Canuto C, Hussaini MY, Quarteroni A, Zang TA. 2007. *Spectral Methods: Evolution to Complex Geometries and Applications to Fluid Dynamics*. Springer: Berlin.

Clark CD. 1993. Mega-scale glacial lineations and cross-cutting ice-flow landforms. *Earth Surface Processes and Landforms* **18**: 1–29.

Clark CD, Meehan RT. 2001. Subglacial bedform geomorphology of the Irish Ice Sheet reveals major configuration changes during growth and decay. *Journal of Quarterly Science* **16**: 483–496.

Clark CD, Hughes ALC, Greenwood SL, Spagnolo M, Ng FSL. 2009. Size and shape characteristics of drumlins, derived from a large sample, and associated scaling laws. *Quaternary Science Reviews* **28**: 677–692.

Creyts TT, Schoof CG. 2009. Drainage through subglacial water sheets. *Journal of Geophysical Research* **114**: F04008.

Dunlop P, Clark CD. 2006. The morphological characteristics of ribbed moraine. *Quaternary Science Reviews* **25**: 1668–1691.

Dunlop P, Clark CD, Hindmarsh RCA. 2008. Bed ribbing instability explanation: testing a numerical model of ribbed moraine formation arising from coupled flow of ice and subglacial sediment. *Journal of Geophysical Research* **113**: F03005.

Fisher TG, Shaw J. 1992. A depositional model for Rogen moraine, with examples from the Avalon Peninsula, Newfoundland. *Canadian Journal of Earth Sciences* **29**: 669–686.

Fowler AC. 2000. An instability mechanism for drumlin formation. In *Deformation of Subglacial Materials*, Maltman A, Hambrey MJ, Hubbard B (eds). Special Publication 176. Geological Society: London; 307–319.

Fowler AC. 2009. Instability modelling of drumlin formation incorporating lee-side cavity growth. *Proceedings of the Royal Society of London A* **465**: 2681–2702.

Fowler AC. 2010a. The stability theory of drumlin formation applied to Newtonian viscous ice of finite depth. *Proceedings of the Royal Society of London A* **466**: 2673–2694.

Fowler AC. 2010b. The formation of sub-glacial streams and mega-scale glacial lineations. *Proceedings of the Royal Society of London A* **466**: 3181–3201. DOI: 10.1098/rspa.2010.0009

Hättestrand C, Kleman J. 1999. Ribbed moraine formation. *Quaternary Science Reviews* **18**: 43–61.

Hindmarsh RA. 1998. The stability of a viscous till sheet coupled with ice flow, considered at wavelengths less than the ice thickness. *Journal of Glaciology* **44**(146): 285–292.

King EC, Hindmarsh RCA, Stokes CR. 2009. Formation of mega-scale glacial lineations observed beneath a West Antarctic ice stream. *Nature Geoscience* **2**: 585–588.

Kleman J, Hättestrand C. 1999. Frozen-bed Fennoscandian and Laurentide ice sheets during the last glacial maximum. *Nature* **402**: 63–66.

Lindén M, Möller P, Adrielson L. 2008. Ribbed moraine formed by subglacial folding, thrust stacking and lee-side cavity infill. *Boreas* **37**: 102–131.

Lundqvist J. 1969. *Problems of the so-called Rogen moraine*. Sveriges Geologiska Undersökning C 648.

Menzies J. 1979. A review of the literature on the formation and location of drumlins. *Earth Science Reviews* **14**: 315–359.

Möller P. 2006. Rogen moraine: an example of glacial re-shaping of pre-existing landforms. *Quaternary Science Reviews* **25**: 362–389.

Möller P. 2010. Melt-out till and ribbed moraine formation, a case study from south Sweden. *Sedimentary Geology* **232**: 161–180.

Patterson CJ, Hooke LH. 1995. Physical environment of drumlin formation. *Journal of Glaciology* **41**: 30–38.

Pelletier JD. 2008. *Quantitative Modeling of Earth Surface Processes*. Cambridge University Press: Cambridge, UK.

Röthlisberger H. 1972. Water pressure in intra- and subglacial channels. *Journal of Glaciology* **11**: 177–203.

Schoof C. 2007a. Pressure-dependent viscosity and interfacial instability in coupled ice–sediment flow. *Journal of Fluid Mechanics* **570**: 227–252.

Schoof C. 2007b. Cavitation in deformable glacier beds. *SIAM Journal on Applied Mathematics* **67**: 1633–1653.

Sugden DE, John BS. 1976. *Glaciers and Landscape*. Edward Arnold: London.

Walder JS, Fowler A. 1994. Channelised subglacial drainage over a deformable bed. *Journal of Glaciology* **40**: 3–15.